Polymer Chemistry

Accepted Manuscript

ROYAL SOCIETY OF CHEMISTRY

www.rsc.org/polymers

Poly(4-Vinylpyridine)-*block*-poly(*N*-acryloylpiperidine) Diblock Copolymers: Synthesis, Self-Assembly and Interaction

Anton H. Hofman, Gert O. R. Alberda van Ekenstein, Albert J. J. Woortman, Gerrit ten Brinke* and Katja Loos*

Department of Polymer Chemistry, Zernike Institute for Advanced Materials, University of Groningen, Nijenborgh 4, 9747 AG Groningen, The Netherlands

*g.ten.brinke@rug.nl and k.u.loos@rug.nl

Abstract

Controlled radical polymerization of 4-vinylpyridine (4VP) and *N*-acryloylpiperidine (API) by the RAFT process allowed preparation of well-defined double hydrogen bond accepting P4VP-*b*-PAPI diblock copolymers. The miscibility of this new monomer pair was studied via a random copolymer blend approach and resulted in a Flory-Huggins interaction parameter $\chi_{4VP,API} \approx 0.03$, which is higher than the commonly used styrene/MMA couple, but lower compared to styrene/isoprene. This value was found to support the bulk phase behavior of a series of diblock copolymers as evidenced by SAXS and TEM. Highly ordered structures, including cylinders, lamellae and spheres, were identified in these materials, even in diblocks of higher molecular weight and broader distribution, while a disordered morphology was indeed observed in a symmetric, low molecular weight analogue.

Introduction

Block copolymers are promising materials for applications in nanotechnology, since they are able to spontaneously form ordered structures at the nano- to mesoscale.[1] Examples include their use in membrane technology,[2] lithography,[3–5] microelectronics,[6] scaffolds for the preparation of ordered organic or inorganic materials[7–10] and even soft photonic crystals.[11] The obtained structure and its domain spacing depend on the composition (f) of the block copolymer and the molecular weight (N), respectively, while the smallest accessible feature size is determined by the Flory-Huggins interaction parameter (χ). Self-assembly of a simple diblock copolymer already allows the preparation of several different morphologies, such as spheres, cylinders, lamellae and bicontinuous network structures,[12] while more complex polymeric architectures (triblocks, multiblocks, star-shaped, comb-shaped, etc.) usually result in more complex phase behavior.[13–15]

Special reaction conditions are required in order to obtain such well-defined block copolymers, which are fulfilled by several living or controlled polymerization techniques available nowadays. Amongst these, living anionic polymerization is superior in sense of controllability and suppression of termination side reactions compared to the more recently introduced radical-based methods.[16] However, due to the high reactivity of the propagating anionic species this type of polymerization is extremely sensitive to moisture and oxygen, has a low monomer compatibility (protic/electrophilic monomers require protecting groups)[17,18] and only a limited number of solvents are known to be applicable. Controlled radical polymerization (CRP) methods solve these deficiencies at the cost of some loss in controllability, but makes it possible to incorporate functionality into the polymeric material without additional protection/deprotection steps. CRP techniques that have proven their worth during the past decade include atom transfer radical polymerization (ATRP),[19] nitroxide mediated polymerization (NMP)[20] and reversible addition-fragmentation chain transfer (RAFT) polymerization.[21]

The last method possesses several advantages over the first two since it was found to be applicable at a high variety of reaction conditions (both temperature and solvent) and compatible with a large library of monomers. These include styrenics, vinylpyridines, (meth)acrylates, (meth)acrylamides and acrylonitrile.[22,23] Furthermore, well-defined amphiphilic di- and tri-

block copolymers can be prepared by careful selection of the chain transfer agent (CTA) and the sequence of monomer addition.[24,25]

The polymerization of 4-vinylpyridine (4VP) by RAFT has been studied thoroughly by many research groups, as the corresponding polymer is an interesting material for several applications, owing to its thermal properties, hydrogen bond accepting capability, pH responsiveness and ability to coordinate to transition metals. P4VP could be prepared with high precision using dithiobenzoate-based RAFT agents, although relatively long reaction times were required for obtaining both high conversions and degree of polymerizations.[26,27] Trithiocarbonate CTAs have indeed been shown to increase 4VP's rate of polymerization, although to our knowledge a proper kinetic investigation has not been reported in literature.[28–30]

The same holds for the controlled polymerization of *N*-acryloylpiperidine (API) by RAFT: polar, but water-insoluble PAPI homopolymers could be synthesized with great precision using dithiobenzoate-based RAFT agents, while a proper kinetic analysis was found to be unavailable at the time of writing.[31] On the other hand, both *N*-substituted[32] and *N,N*-disubstituted acrylamides[33–35] are generally known to be highly compatible with the RAFT method allowing the synthesis of well-defined block copolymers. Indeed, in a previous contribution[36] our group demonstrated the possibility to prepare a low-polydispersity diblock copolymer based on P4VP and PAPI using a trithiocarbonate CTA. Since the reported procedure was very successful and self-assembly of the final product resulted in highly ordered structures, we decided to study the RAFT process of both monomers in more detail and, in addition, aim for asymmetric P4VP-*b*-PAPI block copolymers. Such double hydrogen bond accepting diblock copolymers could also be of particular interest because of their water-insolubility and non-hygroscopic nature, while being fully soluble in many polar organic solvents. Finally, since a thorough investigation of the self-assembly of 4VP/acrylamide block copolymers has not been reported in literature before, a 4VP/API monomer miscibility study based on a random copolymer blend approach will be presented as well.

Experimental section

Materials. α,α'-azobis(isobutyronitrile) (AIBN, Fluka, >98%) was recrystallized twice from methanol. The RAFT agent *S*-dodecyl-*S*'-(isobutyric acid) trithiocarbonate (DIBTTC) was prepared according to literature procedure.[37] 4-vinylpyridine (4VP, Sigma-Aldrich, ≥94.5%) was condensed twice on a high-vacuum line, first from calcium hydride and then from the respective trioctylaluminum treated pale yellow/green solution. The monomer *N*-acryloylpiperidine (API) was synthesized via the route provided by Kobayashi et al.,[38] purified by column chromatography (acetone as eluent) and finally vacuum distilled from finely ground calcium hydride (Acros Organics, ≥91.0%). 1-dodecanethiol (TCI, >95.0%), tricaprylylmethylammonium chloride (Aliquat 336, TCI), carbon disulfide (Acros Organics, ≥99.9%), acryloyl chloride (Sigma-Alrich, ≥97.0%), piperidine (Acros Organics, ≥99.4%, AcroSeal), triethylamine (Sigma-Aldrich, ≥99.5%), *N,N*-dimethylformamide (DMF, Sigma-Aldrich, anhydrous, ≥99.8%), DMF for gel permeation chromatography (Acros Organics, GPC grade), lithium bromide (Acros Organics, anhydrous, ≥99.0%) and trioctylaluminum (25 wt % in hexane, Sigma-Aldrich) were used as received. All other solvents were of analytical grade.

Synthesis of P4VP, PAPI and P4VP-*b*-PAPI by RAFT. A general route for RAFT polymerization of API and 4VP is described below. In a 50 ml round-bottom flask equipped with a Teflon-coated stirring egg, DIBTTC (homopolymers) or P4VP macro-CTA (diblock copolymers) was dissolved in DMF, monomer (4VP or API) was added and finally a calculated amount of AIBN stock solution in DMF was injected via a syringe. Then the flask was connected to a high-vacuum line and after being subjected to at least four freeze-pump-thaw cycles it was backfilled with argon. The reaction was started by submerging the closed flask in a thermostated oil bath at 70 °C. The polymerization was carried out for the time indicated, quenched by rapid cooling using liquid nitrogen and its conversion was determined using ^{1}H-NMR. The solution was diluted with chloroform or DMF, P4VP homopolymers precipitated and reprecipitated into at least a tenfold excess of toluene, PAPI homopolymers into hexane/ether (1/1) and hexane and block copolymers into hexane/ether (1/1) and hexane, respectively. The obtained orange to light yellow powder was dried in a vacuum oven.

Synthesis of P(4VP-*co*-API) random copolymers. Random copolymers of 4VP and API for miscibility studies were prepared by dissolving $2-3$ g monomer and $5-6$ mg AIBN in 3 ml DMF in a 50 ml two-neck flask equipped with a Teflon-coated stirring egg. The solutions were subjected to at least four freeze-pump-thaw cycles and after being backfilled with argon the free radical polymerization was carried out at 80 °C. The reaction was quenched by submerging the flask in liquid nitrogen after 30 min to 1 h. Conversions were kept as low as possible (conversion of 4VP $< 30\%$) in order to avoid composition drift. Copolymers were precipitated into a 30-fold excess of hexane/ether (1/1) containing a small amount of hydroquinone, dissolved in chloroform and reprecipitated into hexane. After drying in a vacuum oven, the random copolymers were obtained as white powders with typical yields of ca. $200-300$ mg.

Sample preparation. Bulk films of the P4VP-*b*-PAPI diblock copolymers were obtained by dissolving 150 mg of the polymer in DMF (max. 2 wt %), followed by casting these solutions into 4 cm Petri dishes. Full evaporation of the solvent in a DMF atmosphere (45 °C) was achieved in approximately one week. Solvent history was removed by annealing the transparent block copolymer films in a vacuum oven for about 5 days at 200 °C.

Ultrathin sections (80 nm) for transmission electron microscopy (TEM) were obtained by microtoming in epoxy (Epofix, Electron Microscopy Sciences) embedded pieces of the polymer films using a Leica Ultracut UCT ultramicrotome equipped with a 35° DiATOME diamond knife. Enhanced contrast for TEM was realized by staining the sections with iodine for 2 to 7 hours.

Samples for SAXS were prepared by pressing small pellets of the previously cast bulk films, followed by thermal annealing at 200 °C for roughly 5 days.

P4VP homopolymer/random copolymer 50/50 wt % blends for miscibility studies were prepared by dissolving equal amounts of the copolymer and homopolymer in chloroform and direct casting of these solution into DSC pans. Each pan contained $8-10$ mg material after evaporation of the solvent. Equilibrium in the melt state was promoted by heating the pans to 200 °C for about one hour. The blends were finally annealed in the glassy state for several days up to weeks in a closed, thermostated, custom-made heating block.

Characterization. Nuclear magnetic resonance (NMR) spectra were recorded on a 400 MHz Varian VXR operating at room temperature using deuterated chloroform ($CDCl_3$) as solvent.

Gel permeation chromatography (GPC) was performed in DMF (containing 0.01 M LiBr) on a Viscotek GPCmax equipped with model 302 TDA detectors, using a guard column

(PSS-GRAM, 10 μm 5 cm) and two analytical columns (PSS-GRAM-1000/30 Å, 10 μm 30 cm) at a flow rate of 1.0 ml·min^{-1}. The columns and detectors were held at 50 °C. Narrow PMMA standards were used for calibration of the system and samples were filtered over a 0.45 μm PTFE filter prior to injection. Molecular weights were calculated by applying a triple detection method (refractive index, viscosity and light scattering) using Viscotec Omnisec software. A predetermined refractive index increment (dn/dc) of 0.153 ml·g^{-1} was used for P4VP homopolymers.[39]

Differential scanning calorimetry (DSC) was carried out on a DSC Q1000 of TA Instruments in the modulated mode (0.5 °C, period 60 s) by heating the samples to 200 °C and cooling to 60 °C at a rate of 2 °C·min^{-1}, unless stated differently. Copolymer miscibility was judged by looking at the first heating cycle, while the second was used for the determination of glass transitions.

Thermogravimetric analysis (TGA) was performed on a Perkin Elmer TGA 7. Thermal stability of the co- and homopolymers was examined by heating the samples to 900 °C at a rate of 10 °C·min^{-1} or held at a constant temperature for a certain amount of time (Supporting Information).

Small-angle X-ray scattering (SAXS) measurements were carried out at the Dutch-Belgian Beamline (DUBBLE), station BM26B of the European Synchrotron Radiation Facility (ESRF) in Grenoble, France.[40,41] The sample-to-detector distance (Dectris Pilatus 1M) of the setup was ca. 5.0 m. The scattering vector q is defined as $q = 4\pi/\lambda \sin\theta$ with 2θ being the scattering angle and λ the wavelength of the X-rays (1.03 Å). The acquisition time was 5 minutes per sample.

Sections of the iodine stained diblock copolymers were analyzed on a Philips CM12 transmission electron microscope operating at an accelerating voltage of 120 kV. TEM images were recorded on a Gatan slow-scan CCD camera.

Results and discussion

Synthesis of P4VP, PAPI and P4VP-*b*-PAPI

Appropriate selection of the CTA (both R- and Z-group) is one of the most important criteria for achieving successful RAFT polymerization.[42] In addition, the ratio thermal initiator/CTA should be as low as possible in order to suppress termination side reactions, although it should still be sufficiently high for obtaining a reasonable rate of polymerization. In other words, an optimum exists between the two concentrations that reflects both the rate and controllability. Compared to dithioester-based CTAs, trithiocarbonates have been shown to have superior properties with respect to their chain transfer efficiency, allowing a lower concentration of thermal initiator for maintaining a similar rate of polymerization. Furthermore, this type of CTA is known to be compatible with a larger library of monomers, to give substantially less rate retardation, is less prone to hydrolytic degradation and is easier to synthesize.[23]

Trithiocarbonates have indeed been successfully employed in the synthesis of well-defined polystyrenes[25,37] and polyacrylamides,[33–35] although for both 4VP and API previous reports lacked a proper kinetic analysis. For this reason we first looked into the synthesis of both homopolymers in more detail, before moving towards the self-assembly of RAFT-synthesized P4VP-*b*-PAPI diblock copolymers.

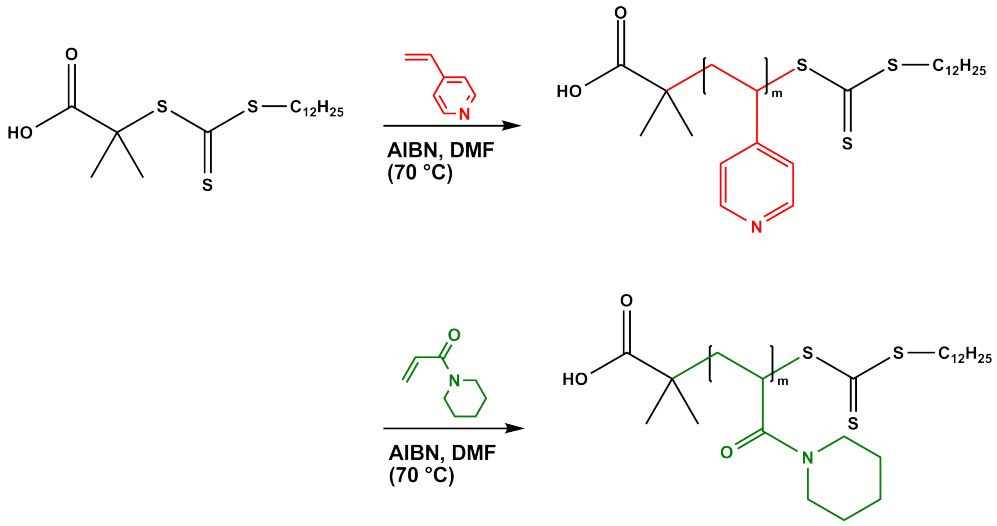

Scheme 1: Synthesis pathways for the preparation of P4VP and PAPI homopolymers by RAFT.

For the kinetics of the RAFT polymerization of 4VP and API (Scheme 1) a large stock solution, containing AIBN, DIBTTC, monomer and DMF, was subjected to several freeze-pump-thaw cycles and then divided over four different flasks. Each reaction mixture was heated at 70 °C for a certain amount of time, subsequently quenched by submerging the flask into liquid nitrogen and conversions were determined by ^{1}H-NMR by comparing the integral values of monomer and polymer.

A linear relationship (Equation 1, [M] is the monomer concentration) was found over 4VP's entire conversion range in the pseudo first-order rate plot presented in Figure 1a, meaning that termination and other side reactions were suppressed effectively by the CTA. In addition, molecular weights as determined by GPC follow the linear theoretical trend given by Equation 2 with great accuracy (m_0 is the molecular weight of the monomer), while polydispersities remained well below 1.1 (Figure 1b). From this data it is clear that addition of DIBTTC allowed controlled polymerization of 4VP by RAFT.

$$\ln\left(\frac{[\mathrm{M}]_0}{[\mathrm{M}]}\right) = k_{\mathrm{app}} \cdot t \tag{1}$$

$$M_n = \frac{[\mathrm{M}]_0}{[\mathrm{DIBTTC}]} \cdot m_0 \cdot \mathrm{Conv.} + m_{\mathrm{DIBTTC}} \tag{2}$$

Pseudo first-order kinetics were observed in the DIBTTC-mediated polymerization of API as well (Figure 2a). A linear increase of the GPC-determined molecular weights with conversion was found over the full range and moreover, polydispersity indices never exceeded a value of 1.1 (Figure 2b). Compared to the polymerization of 4VP, higher reaction rates were observed, e.g. 77% monomer conversion was measured after only two hours, presumably caused by API's inability to stabilize the propagating radical by resonance. Despite this high rate, the RAFT process still yielded PAPI homopolymers with predictable molecular weights and narrow distributions.

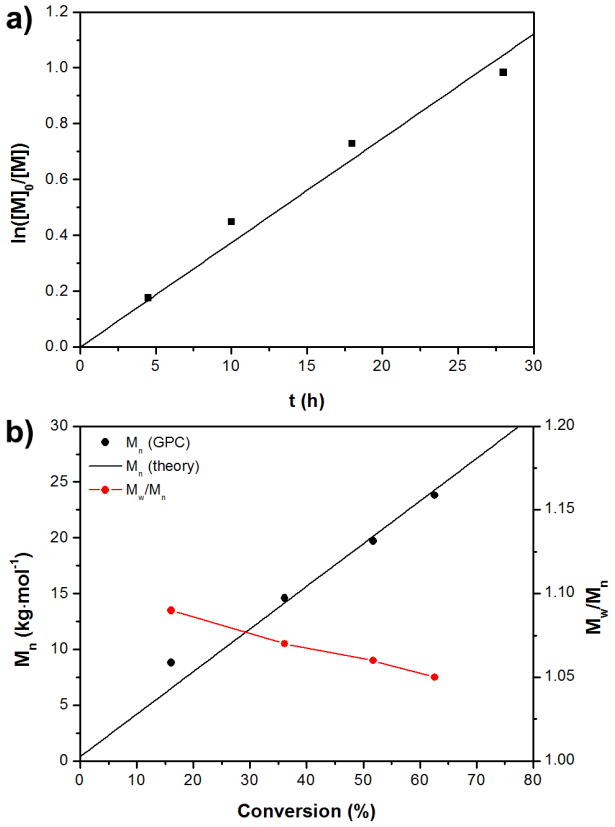

Figure 1: Pseudo first-order rate plot (a) and evolution of molecular weight and polydispersity of P4VP with conversion (b). Reaction conditions: [AIBN] = 1.2 mM, [DIBTTC] = 10 mM and [4VP] = 3.7 M.

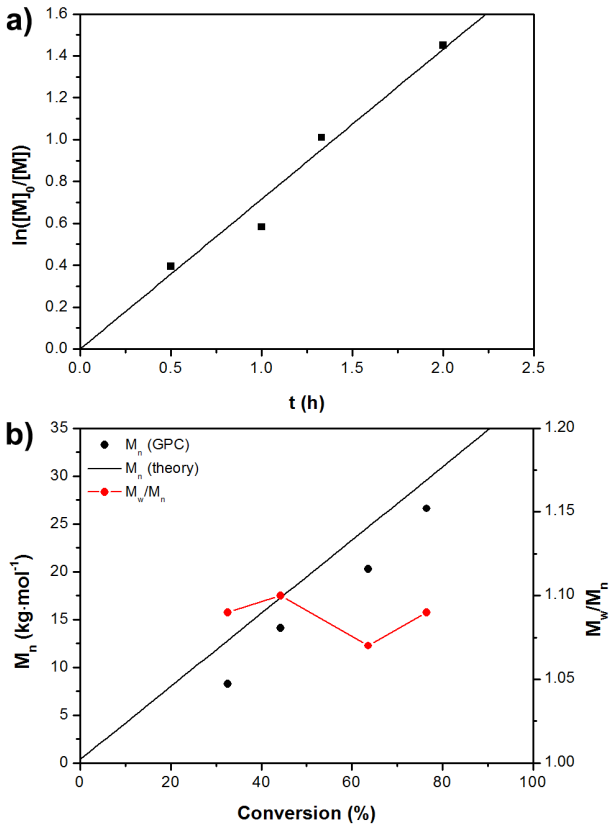

Figure 2: Pseudo first-order rate plot (a) and evolution of molecular weight and polydispersity of PAPI with conversion (b). Reaction conditions: [AIBN] = 0.76 mM, [DIBTTC] = 7.4 mM and [API] = 2.0 M.

Macro-CTA	[DIBTTC][a]	[AIBN][a]	[AIBN]/[DIBTTC]	[4VP][b]	t_R [c]	Conv. (%)	$M_{n,theory}$ [d]	$M_{n,GPC}$ [d]	M_w/M_n
P4VP-8k	46	1.5	1/31	4.8	21	61.4	7.08	7.95	1.17
P4VP-14k	19	1.0	1/18	3.8	21	57.4	12.8	14.2	1.13
P4VP-29k	9.8	1.0	1/10	3.7	20	66.3	26.5	28.8	1.05
P4VP-40k	5.2	0.70	1/7.4	3.8	25	49.3	38.3	40.3	1.16
P4VP-55k	5.9	0.69	1/8.6	5.6	20	53.7	53.7	55.0	1.07

Table 1: Overview of P4VP macro-CTAs synthesized by RAFT in DMF at 70 °C. [a] DIBTTC and AIBN concentrations are in mM, [b] 4VP in M, [c] reaction times (t_R) in hours and [d] molecular weights in kg·mol^{-1}.

Similar to living ionic polymerization techniques, the sequence of monomer addition for the preparation of block copolymers (BCPs) is very important in RAFT polymerization as well, because the transfer efficiency of the macro-CTA to the second monomer significantly affects the corresponding diblock copolymer's molecular weight distribution. Such instantaneous re-initiation can only be achieved by starting the diblock copolymer synthesis with the monomer with highest leaving ability. In other words, the first monomer should be the one with the greater stability of the re-initiating radical, or lowest reactivity.[22] For this reason P4VP-*b*-PAPI diblock copolymers could be synthesized by starting the reaction with a trithiocarbonate end-capped P4VP homopolymer (Scheme 2). In order to be able to prepare BCPs with different molecular weights and compositions, first several P4VP macro-CTAs were prepared by varying the concentrations of DIBTTC, 4VP and AIBN. This led to P4VP homopolymers with molecular weights ranging from 7.95 to 55.0 kg·mol^{-1} and polydispersity indices (PDIs) smaller than 1.2 (Table 1).

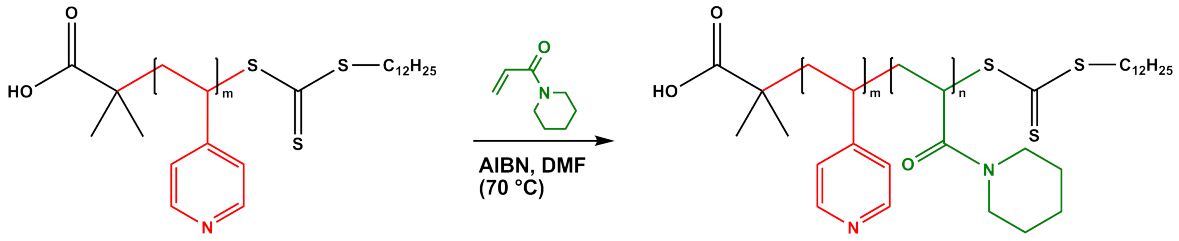

Scheme 2: Synthesis of P4VP-*b*-PAPI diblock copolymers by the RAFT process, starting from a P4VP macro-CTA.

As the polymerization of API was observed to be very fast compared to 4VP, this finding was utilized for the preparation of the diblock copolymers: we aimed for a certain PAPI block length (i.e. diblock composition) by addition of the required amount of monomer provided that reaction would go to full conversion. The concentration of AIBN was kept as low as possible in order to maintain control over the polymerization ([AIBN]/[DIBTTC] < 1/7.5), while a decent rate of polymerization was achieved by decreasing the amount of solvent (DMF) in case [AIBN] and [API] would have been too low. According to ^{1}H-NMR spectra of aliquots taken from the quenched reaction mixture, this method resulted in API conversions between 65 and 98% (Table 2).

BCP	[P4VP]^a	[AIBN]^a	[AIBN]/[P4VP]	[API]^b	t_R ^{c}	Conv. (%)
P4PA80k-10	5.5	0.48	1/12	2.5	20	98
P4PA131k-22	3.3	0.41	1/7.7	2.3	20	91
P4PA61k-23	7.4	0.80	1/9.3	2.5	19	97
P4PA129k-31	3.3	0.41	1/8.1	2.3	20	87
P4PA57k-47	7.1	0.76	1/9.4	1.8	17	83
P4PA78k-70	7.1	0.80	1/8.9	1.4	22	70
P4PA48k-83	10	1.1	1/9.5	0.97	19	65

Table 2: Reaction conditions for the preparation of P4VP-*b*-PAPI diblock copolymers. ^{a} P4VP and AIBN concentrations are in mM, ^{b} API in M and ^{c} reaction times (t_R) in hours.

Several P4VP-*b*-PAPI diblock copolymers with varying length and composition were prepared by following the described route (Table 3). In the codes used (P4PAxk-y), x represents the molecular weight in kg·mol^{-1} and y the P4VP weight percentage. Compositions (f_{P4VP}, weight fractions) were calculated by comparing the integral regions of P4VP and PAPI in ^{1}H-NMR (Figure S1, P4PA129k-31), while total molecular weights (M_n) were determined by using this value and the GPC-resolved molecular weight of the P4VP macro-CTA ($M_{n,\mathrm{P4VP}}$). Another estimation for the molecular weight was made by looking at the conversions abstracted from ^{1}H-NMR spectra of the reaction mixture ($M_{n,\mathrm{PAPI\,(conv.)}}$). Although this method is less accurate compared to the previously discussed one based on the P4VP macro-CTA, it is interesting to see that the numbers are similar. GPC showed that in all experiments the P4VP macro-CTAs were extended properly, since maxima shifted to lower retention volumes after polymerization of API (Figure S2, P4PA129k-31). Significant tailing on the low molecular weight side (due to early termination) was found to be absent in most reactions. Fast conversion of API monomer allowed the synthesis of various high molecular weight P4VP-*b*-PAPI diblock copolymers by RAFT ($0.10 < f_{\mathrm{P4VP}} < 0.83$, up to 131 kg·mol^{-1}) with narrow distributions ($M_w/M_n < 1.4$), while even lower PDIs ($M_w/M_n < 1.2$) were obtained for smaller diblocks (up to 80 kg·mol^{-1}).

Self-assembly of P4VP-*b*-PAPI

Diblock copolymers are known to form ordered nanometer-sized structures spontaneously if the product of the Flory-Huggins interaction parameter χ and the number of segments N is sufficiently high ($\chi N > 10.5$), i.e. high molecular weights are required for weakly interacting monomer pairs. If this condition is met, the type of morphology formed (spheres, cylinders, lamellae, gyroid, etc.) depends on the composition of the block copolymer.

The phase behavior of thermally annealed bulk films of the P4VP-*b*-PAPI diblock copolymers (Table 4) was investigated thoroughly using DSC, SAXS and TEM. In all copolymers two glass transitions were observed (around 128 and 153 °C for PAPI and P4VP respectively)

BCP	$M_{n,\mathrm{P4VP}}$ [a]	$M_{n,\mathrm{PAPI\,(conv.)}}$ [a]	$M_{n,\mathrm{PAPI}}$ [a]	M_n [a]	f_{P4VP} [b]	M_w/M_n
P4PA80k-10	7.95	62.6	71.8	79.8	0.10	1.18
P4PA131k-22	28.8	92.4	102	131	0.22	1.34
P4PA61k-23	14.2	45.2	46.8	61.0	0.23	1.14
P4PA129k-31	40.3	85.0	88.8	129	0.31	1.26
P4PA57k-47	28.8	29.1	30.0	56.5	0.47	1.06
P4PA78k-70	55.0	20.0	23.2	78.2	0.70	1.05
P4PA48k-83	40.3	8.69	8.10	48.4	0.83	1.12

Table 3: [a] Molar masses (kg·mol^{-1}) and [b] composition data (weigth fractions) of the RAFT-synthesized P4VP-*b*-PAPI diblock copolymers.

BCP	M_n [a]	M_w/M_n	f_{P4VP} [b]	d_{SAXS} [c]	d_{FT} [c]	χN [d]
P4PA80k-10	79.8	1.18	0.10	N/A	30	24
P4PA131k-22	131	1.34	0.22	61	61	39
P4PA61k-23	61.0	1.14	0.23	31	34	18
P4PA129k-31	129	1.26	0.31	74	81	39
P4PA57k-47	56.5	1.06	0.47	37	55	17
P4PA78k-70	78.2	1.05	0.70	43	40	23
P4PA48k-83	48.4	1.12	0.83	N/A	24	15

Table 4: Overview of P4VP-*b*-PAPI diblock copolymers: molecular weights, composition, self-assembly and interaction. [a] Molecular weights are in kg·mol^{-1}, [b] fractions denote weight fractions, [c] distances are in nm, [d] $\chi_{\mathrm{4VP,API}}$ was assumed to be 0.03 and $N = M_n$ / 100 g·mol^{-1}.

indicating that these were phase separated, except for the very asymmetric block copolymers ($f_{P4VP} < 0.22$ and $f_{P4VP} > 0.70$) since the weight of their minority block was simply too small to be observed by DSC (Figure S3, P4PA129k-31). It should be remarked that all fractions in this paper denote weight fractions, while volume fractions are needed for a proper comparison with theoretical models. However, volume fractions could unfortunately not be calculated, since the density of PAPI is unknown. On the other hand, densities of P4VP and PAPI are expected to be rather similar, as densities of amorphous polyvinylpyridines and polyalkylacrylamides are known to be in between 1.0 and 1.1 g·cm^{-3}.[39]

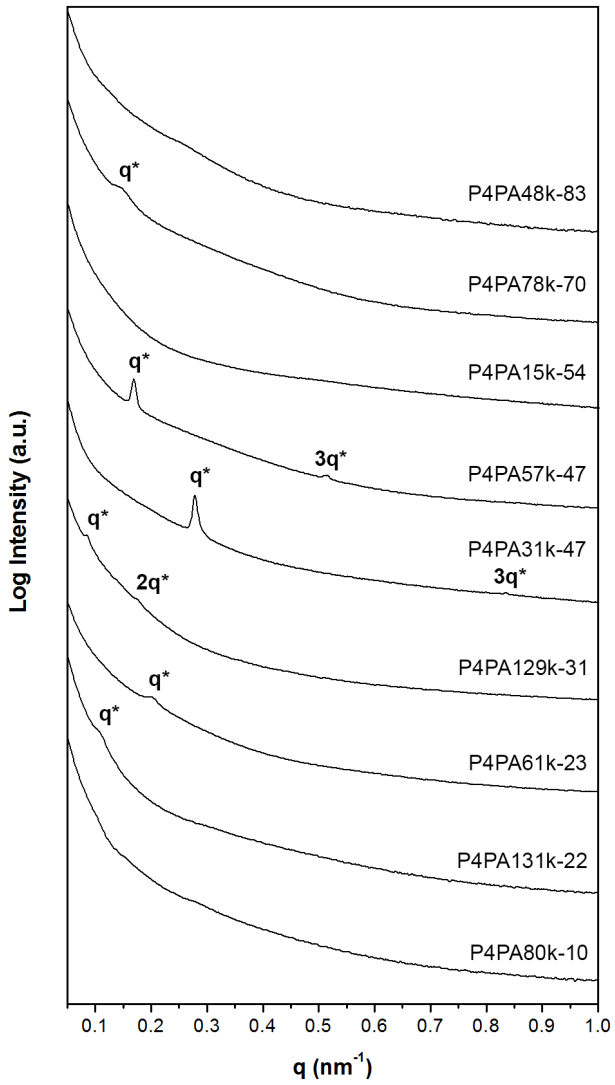

Figure 3: Room temperature SAXS profiles of P4VP-*b*-PAPI diblock copolymers.

Self-assembly of each BCP will be discussed with increasing fraction of P4VP, starting with P4PA80k-10 (the first number represents the copolymer molecular weight in kg·mol^{-1}, the second the weight fraction P4VP). When compared to the mean-field phase diagram for symmetric diblock melts,[43] based on the weight fraction a spherical or disordered morphology

would be expected, depending on the Flory-Huggins interaction parameter. In SAXS (Figure 3) no scattering maxima could be observed, while a TEM image (Figure 4a) of an iodine stained section (P4VP appears dark) shows a micellar-like structure. Such a morphology could indicate both a spherical or disordered structure, but without proper SAXS data no conclusions should be drawn from TEM only. Interestingly though, the Fourier transformation (FT) of this image (inset) would imply the presence of a 30 nm periodic structure.

The TEM micrograph of P4PA131k-22 (Figure 4b) clearly demonstrates the expected cylindrical structure: both orientations (parallel and perpendicular) of hexagonally packed P4VP cylinders embedded in a PAPI matrix are clearly present ($d_{\mathrm{FT}} \approx 61$ nm). Its SAXS pattern in Figure 3 on the other hand only shows a faint shoulder at $q = 0.10$ nm^{-1} ($d = 61$ nm). The absence of higher order scattering maxima does not allow a detailed analysis of the type of structure in this BCP.

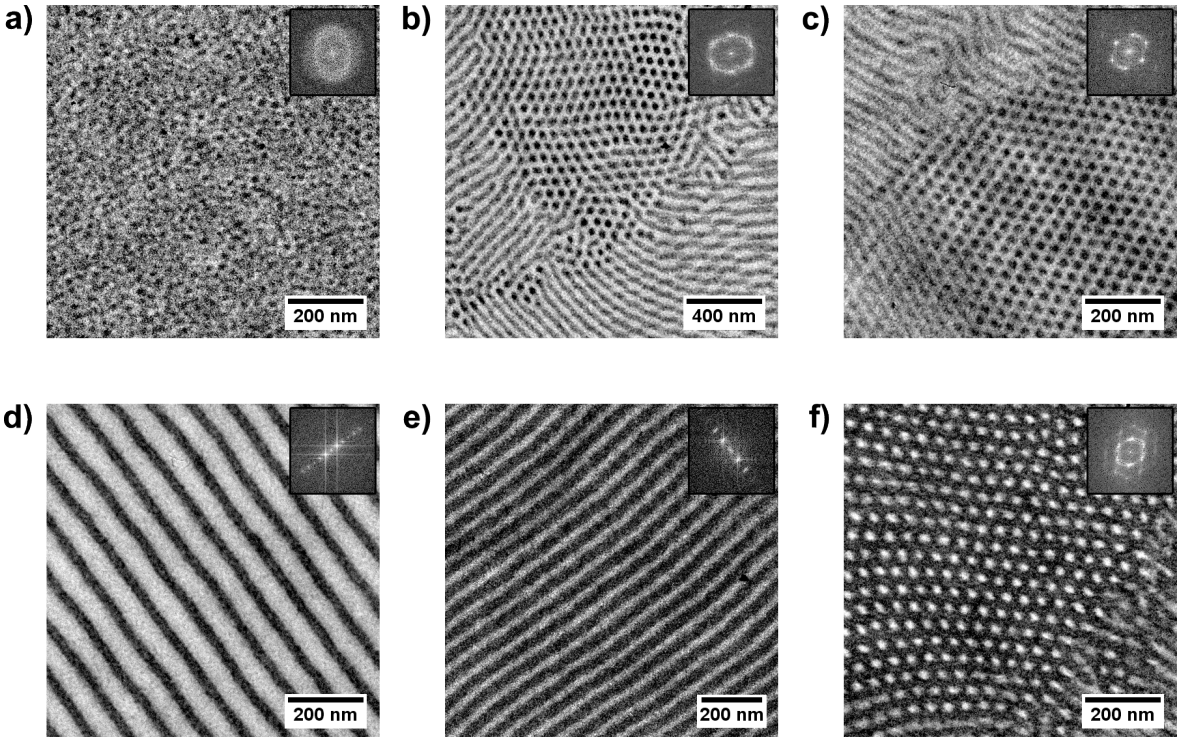

Figure 4: Transmission electron micrographs of P4VP-*b*-PAPI diblock copolymers. P4VP appears dark due to staining with iodine. The inset shows the corresponding Fourier transformation. P4PA80k-10 (a), P4PA131k-22 (b), P4PA61k-23 (c), P4PA129k-31 (d), P4PA57k-47 (e) and P4PA78k-70 (f).

P4PA61k-23 only differs from P4PA131k-22 with respect to its molecular weight, resulting in indeed the formation of P4VP cylinders, although at a smaller length scale (Figure 4c, $d_{\mathrm{FT}} \approx 34$ nm). Despite the absence of higher order scattering maxima, similar to P4PA131k-22, this length scale ($d = 31$ nm) is confirmed by the single peak found in SAXS (Figure 3).

In contrast to the previous P4VP-*b*-PAPI diblock copolymers, the SAXS profile of P4PA129k-31 shows two relatively weak signals with a ratio of $1q^* : 2q^*$ ($q^* = 0.085$ nm^{-1}, $d = 74$ nm). This data still provides insufficient information for concluding anything about its morphol-

ogy, but analysis of stained sections by TEM demonstrates its self-assembly into very well ordered lamellae (Figure 4d, $d_{FT} \approx 81$ nm). Although this BCP would be expected to give a cylindrical structure upon microphase separation (based on the theoretical phase diagram), f_{P4VP} is situated just on the border of the lamellae to cylinders transition. If the density of PAPI would be assumed to be slightly higher than P4VP, its composition would certainly shift into the lamellar region. In addition, P4PA129k-31's asymmetry is well reflected by the difference in layer thickness: the bright PAPI lamellae are roughly twice as large compared to the dark, stained P4VP lamellae. Finally, this particular block copolymer demonstrates the ability to form highly ordered structures with large grain sizes (Figure S8) despite its relatively broad molecular weight distribution ($M_w/M_n = 1.26$).

Further increase of the amount of P4VP resulted in an almost symmetrical diblock copolymer: P4PA57k-47. Its diffraction pattern displays two scattering maxima with a ratio of $1q^* : 3q^*$ ($q^* = 0.17$ nm^{-1}, $d = 37$ nm), still insufficient for a proper structural analysis. Lamellae are indeed found in TEM (Figure 4e, $d_{FT} \approx 55$ nm). Based on the observed morphology a second order reflection would be expected in SAXS, although it is generally known that even order reflections are absent for symmetry reasons in lamellar-forming diblocks in which the sublayers are of equal thickness.[44] Also the d-spacing as obtained by SAXS and TEM was found to be quite different ($\Delta d = 18$ nm). It is presumably caused in the microtoming step during which the lamellae are not oriented perfectly perpendicular to the knife. This would result in the structure appearing larger than it actually is. For this reason the layer thickness as identified by SAXS is assumed to be the real value.

Self-assembly of an asymmetric BCP, rich in P4VP (P4PA78k-70) gave rise to the expected inverted cylindrical structure, i.e. PAPI cylinders were embedded in a P4VP matrix (Figure 4f, $d_{FT} \approx 40$ nm). An almost identical length scale could be abstracted from SAXS (43 nm), but similar to the asymmetric polymers poor in P4VP only a shoulder could be observed (Figure 3).

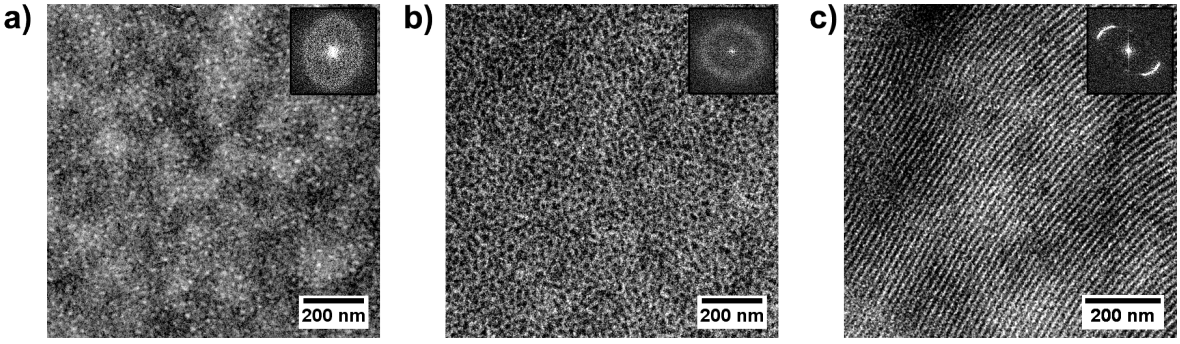

Figure 5: Room temperature TEM images of P4PA48k-83 (a), P4PA15k-54 (b) and P4PA31k-47 (c) after being stained with iodine. Inset shows their corresponding Fourier transformation.

One would expect a spherical morphology for the copolymer with the shortest PAPI block (P4PA48k-83). While SAXS did not show any strong scattering signals, a micellar-like structure could be observed in TEM (Figure 5a, $d_{FT} \approx 24$ nm), similar to P4PA80k-10, but with inverted contrast. Although this particular copolymer could still be situated in the disordered state, most sphere-forming BCPs show comparable phase behavior in TEM, even when

multiple scattering maxima are visible in SAXS.[45] Not many TEM images of well-ordered spheres have been reported in literature.

Regardless of the observed equilibrium structure, all P4VP-*b*-PAPI diblock copolymers have a low scattering intensity in SAXS in common. Quite some of these materials show highly ordered morphologies according to TEM (Figure S5-S11), in most cases even better than the well-studied PS-*b*-PI example,[46,47] but less defined SAXS patterns. Contrast in SAXS is not only determined by the quality of the structure (structure factor), it also depends on the so-called form factor whose magnitude is proportional to the square of the electron density difference. The product of these two factors determines the overall intensity. In other words, a perfectly aligned structure could still yield zero scattering in case the electron density of both phases is identical. Although the density of PAPI is unknown, and therefore its electron density as well, based on the observed phase behavior by TEM, it is very likely the difference between P4VP and PAPI is relatively small.

Finally, it is impressive to see that even with relatively broad molecular weight distributions, compared to living anionic polymerization techniques ($M_w/M_n \approx 1.3$, P4PA131k-22 and P4PA129k-31), the block copolymers were still able to form highly ordered structures (cylinders and lamellae, respectively). Indeed, both theoretical and experimental studies have previously demonstrated that systems with a higher polydispersity can still form ordered nanostructures. Observed differences included changes in order-disorder transition temperature, domain size, interfacial thickness and unexpected phase transitions,[48] while macrophase separation has only been observed in multicomponent blends.[49]

Determination of $\chi_{\mathbf{4VP,API}}$

Monomer miscibility is frequently described using the Flory-Huggins interaction parameter (χ): positive values indicate an unfavorable enthalpic contribution to the Gibbs free energy of mixing, while a negative value would indicate some kind of favorable interaction between the monomer pair (e.g. hydrogen bonding). For a binary system both entropic and enthalpic contributions to the Gibbs free energy of mixing per segment (Δg_m) are included in Equation 3. Here φ represents the volume fraction of component 1 and N_i the segment length of a monodisperse component i. As the chain-like architecture of polymers ($N_i > 100$) is known to cause a significant reduction of the gain in entropy upon mixing, a small positive χ-parameter would already result in macrophase separation in the case of homopolymer blends or microphase separation in BCP melts.[50]

$$\frac{\Delta g_m}{k_B T} = \frac{\varphi}{N_1} \ln \varphi + \frac{1-\varphi}{N_2} \ln(1-\varphi) + \chi_{\text{eff}}\, \varphi\, (1-\varphi) \tag{3}$$

Since the 4VP/API monomer couple described in the previous section has not been studied before and self-assembly of the synthesized P4VP-*b*-PAPI diblock copolymers led to well-ordered mesomorphic structures, we were very interested in its interaction parameter ($\chi_{\text{4VP,API}}$). Several methods have been developed for the experimental estimation of χ during the past decades. Examples of these include contact angle measurements (polymer PA on a surface of polymer PB),[51] neutron reflectometry (interfacial width in PA/PB blends),[52]

temperature-resolved SAXS (order-disorder transition of a PA-*b*-PB diblock copolymer)[53] or via calculations based on solubility parameters.[54]

In this contribution however, a random copolymer blend approach was applied as it was proven to be very effective for various monomer pairs.[55–58] The idea behind this method relies on the principle that even blends of oligomeric analogues of both PA and PB homopolymers are highly likely to phase separate, making it impossible to determine the corresponding interaction parameter. When switching to a blend of PA and a random copolymer P(A_x-*co*-B_{1-x}) miscibility will be observed for a certain volume fraction x.

$$\chi_{\text{eff}} = (1-x)^2\chi_{\text{AB}} \tag{4}$$

According to a mean-field analysis the effective interaction parameter χ_{eff} (copolymer-homopolymer combination) can be expressed in terms of copolymer composition x and interaction parameter of the pure components χ_{AB} (Equation 4).[59–61] For a specific value of x, χ_{AB} can subsequently be calculated using the expression for χ at the critical point (χ_c, Equation 5). In other words, for miscible blends this will yield $\chi_c > (1-x)^2\chi_{\text{AB}}$, while a phase separated blend will give $\chi_c < (1-x)^2\chi_{\text{AB}}$. By adjusting the copolymer composition or the molecular weight of either of the components this procedure will result in an upper and lower boundary for χ_{AB}. N_{w1} and N_{w2} are the weight average segment lengths of the copolymer and homopolymer, respectively (weight averages are used in order to include the polydisperse nature of both compounds).

$$\chi_c \cong \frac{1}{2}\left(\frac{1}{\sqrt{N_{w1}}} + \frac{1}{\sqrt{N_{w2}}}\right)^2 \tag{5}$$

Four P(4VP-*co*-API) random copolymers were synthesized by free radical polymerization of a DMF-based solution containing AIBN as initiator, 4VP and API. The weight fraction 4VP f_{P4VP} in the copolymers (P4-*co*-PAz, $z = f_{\text{P4VP}}\cdot 100\%$) could be adjusted by starting with a different 4VP/API monomer ratio (Table 5). The amount of built-in 4VP was always found to be higher than its feed, which is expected since in contrast to API the propagating radical of 4VP can be stabilized via resonance, resulting in favored addition of the latter. Conversions were kept as low as possible in order to avoid composition drift, although in some cases 4VP reached a conversion of over 30%. Still single, sharp glass transitions (T_g) were identified in these copolymers, increasing with f_{P4VP}.

For the miscibility study all four copolymers were mixed with three P4VP homopolymers, each with a different molecular weight: M_w = 9.3 kg·mol^{-1} (P4VP-9k), 16.1 kg·mol^{-1} (P4VP-16k) and 58.8 kg·mol^{-1} (P4VP-59k) (Table 1). Usually miscibility can be judged by performing a DSC measurement: the presence of two T_gs would suggest a macrophase separated blend, while a single one would indicate miscibility. When the difference between the T_gs of both homopolymers is relatively small or a copolymer with a large value of x (i.e. it differs only slightly from pure PA) is used for analysis, this method is no longer applicable. For this reason we immediately went to a procedure based on enthalpy recovery of samples annealed in the glassy state.[62,63] With this approach, a phase separated thermally aged blend will show two enthalpy recovery peaks in a DSC heating scan, while a homogeneous blend will exhibit only a single enthalpy relaxation maximum.

Copolymer	4VP feed (%)	4VP conv. (%)[a]	f_{P4VP} [a]	T_g [b]	M_w [c]	M_w/M_n
P4-*co*-PA42	20	30	0.42	126	92.8	1.86
P4-*co*-PA55	30	35	0.55	134	90.1	1.94
P4-*co*-PA68	45	23	0.68	141	101	1.76
P4-*co*-PA75	55	28	0.75	146	105	1.66

Table 5: Reaction conditions, molecular weights, compositions and glass transition temperatures of P(4VP-*co*-API) random copolymers. [a] Conversions and compositions (weight fractions) were determined by ^{1}H-NMR, [b] glass transitions by DSC (°C) and [c] molecular weights by GPC (kg·mol^{-1}).

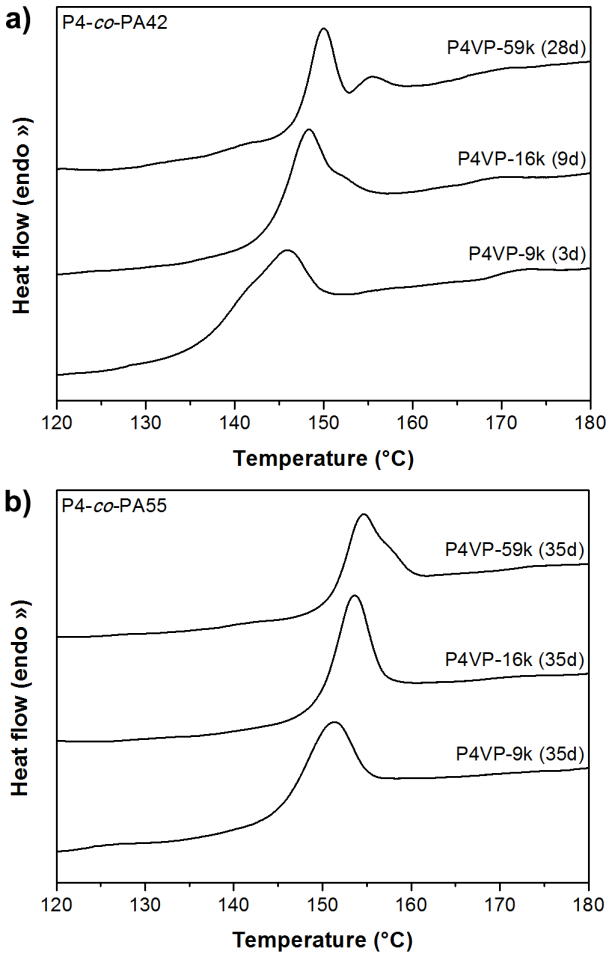

Figure 6: First DSC heating scans of P4VP homopolymer/P4-*co*-PA42 (a, 118 °C) and P4-*co*-PA55 (b, 125 °C) copolymer blends annealed in the glassy state for the times indicated (in days).

Copolymer	P4VP-9k	P4VP-16k	P4VP-59k
P4-*co*-PA42	> 0.028	> 0.019	> 0.008
P4-*co*-PA55	< 0.046	< 0.031	> 0.014
P4-*co*-PA68	< 0.089	< 0.059	< 0.026
P4-*co*-PA75	< 0.145	< 0.096	< 0.042

Table 6: Calculated $\chi_{4VP,API}$ interaction parameters based on miscibility of P(4VP-*co*-API) copolymer/P4VP homopolymer blends.

All samples were aged for several days up to weeks at approximately 10 to 15 °C below the lowest glass transition of the blend. Figure 6a demonstrates the DSC heating scans of P4-*co*-PA42-containing blends after thermal annealing in the glassy state. The two clear maxima (P4VP-59k) or shoulder-containing peaks (P4VP-9k and P4VP-16k) imply macrophase separation to have occurred in these blends. A minimum value for $\chi_{4VP,API}$ could then be calculated as following, using P4VP-59k as example. Since this particular blend was phase separated, the effective interaction parameter is larger than the parameter at the critical point, i.e. $\chi_{eff} > \chi_c$. The segment length of both the homopolymer ($N_{w2} = 588$) and copolymer ($N_{w1} = 928$) was estimated by dividing the molecular weight by 100 g·mol^{-1}. This assumes equal density (1 g·cm^{-3}) and segment volume (166 Å^3) for P4VP and PAPI. An effective interaction parameter could subsequently be obtained by applying Equation 5 ($\chi_{eff} > 0.003$). By inserting the weight fraction x of P4VP ($f_{P4VP} = 0.42$) into Equation 4, this procedure finally resulted in a value for the true interaction parameter: $\chi_{4VP,API} > 0.008$.

From the blends containing a copolymer slightly richer in P4VP (P4-*co*-PA55) only the P4VP-59k-based mixture was found to macrophase separate (Figure 6b) after thermal treatment (up to 35 days). With this available data (Table 6) already a narrow window for $\chi_{4VP,API}$ could be developed as provided by Inequality 6.

$$0.028 < \chi_{4VP,API} < 0.031 \tag{6}$$

Additional copolymer blends with even higher fractions of P4VP were studied as well. None were found to phase separate according to DSC (Figure S12), although based on the previous results, P4VP-59k/P4-*co*-PA68 should have phase separated ($\chi_{4VP,API} > 0.026$). The absence of a clear shoulder or second peak in the heating curve could be caused by insufficiently long thermal aging (40 days) or the relaxation times of both polymers are simply too similar. Compared to other well-studied monomer couples, this interaction parameter ($\chi_{4VP,API} \approx 0.03$) is rather low. It is still slightly higher than styrene/MMA ($\chi_{S,MMA} \approx 0.02$),[64] but smaller than for instance styrene/isoprene ($\chi_{S,I} \approx 0.07$),[64] styrene/2-vinylpyidine ($\chi_{S,2VP} \approx 0.1$) and styrene/4-vinylpyridine ($\chi_{S,4VP} \approx 0.3$).[56] One should however always be aware of the fact that the Flory-Huggins interaction parameter is temperature dependent, mostly inversely proportional. Hence, $\chi_{4VP,API}$ is only valid in the region $150 - 200$ °C, i.e. in between the highest glass transition and the annealing temperature.

Evaluation of $\chi_{4VP,API}$

The P4VP-*b*-PAPI diblock copolymer phase behavior was further analyzed by calculation of the product χN, assuming $\chi_{4VP,API} \approx 0.03$ and $N \approx M_n$ / 100 g·mol^{-1}. According to the obtained values illustrated in Table 4, all BCPs are well within the intermediate segregation regime ($10.5 < \chi N < 100$). Due to the low weight fraction of some of the spherical forming block copolymers (P4PA80k-10 and P4PA48k-83), these polymers could still be located in the disordered region of the theoretical phase diagram as proposed by Matsen and coworkers.[43] However, without proper SAXS data, unfortunately no conclusions can be drawn about their equilibrium structure from TEM images only.

Finally, in order to be able to confirm the χ-parameter obtained from our random copolymer approach, two additional symmetric low molecular weight diblock copolymers were prepared. Based on their composition a lamellar structure should be formed, although insufficiently strong segregation could result in a disordered melt. TEM micrographs of thermally annealed bulk films are displayed in Figure 5 (b and c). Indeed, as expected a highly disordered morphology can be observed for P4PA15k-54 ($\chi N \approx 4.4$) and is confirmed by SAXS due to the absence of any Bragg diffraction (Figure 3). P4PA31k-47 on the other hand, which is just on the border of microphase separation ($\chi N \approx 9.2$), still shows an ordered lamellar structure ($d = 23$ nm). Small uncertainties that were included throughout the complete analysis, such as the assumption of equal densities for P4VP and PAPI, the determination of molecular weights by GPC, estimation of composition by NMR and the use of weight instead of volume fractions, could account for this slightly deviating behavior. According to the self-assembly of these BCPs the order of magnitude of $\chi_{4VP,API}$ is however correct and furthermore, its size is undoubtedly situated in between $\chi_{S,MMA}$ and $\chi_{S,I}$.

Conclusions

Pseudo first-order kinetics and linear increase of the molecular weight with conversion were observed in the polymerization of both 4VP and API by RAFT, indicating the controlled nature of the reactions. Fast propagation of API compared to 4VP allowed the synthesis of various P4VP-*b*-PAPI diblock copolymers with low polydispersities, predictable compositions and predictable molecular weights, starting from a P4VP macro-CTA.

All classical morphologies (spheres, cylinders and lamellae) were identified in the bulk material as evidenced by TEM and SAXS, although their scattering intensity was found to be rather low, presumably caused by a small electron density difference. In addition, even diblocks with higher molecular weights ($M_n > 100$ kg·mol^{-1}) and broader distributions ($M_w/M_n \approx 1.3$) still demonstrated very well ordered cylindrical or lamellar structures.

An estimation for the monomer miscibility was performed by determination of the Flory-Huggins interaction parameter using a random copolymer blend approach. The from these miscibility tests obtained value for the χ-parameter ($\chi_{4VP,API} \approx 0.03$) supports the previously observed BCP self-assembly and furthermore, is positioned in between the interaction parameters of the well-studied styrene/MMA and styrene/isoprene systems. Besides that, the phase behavior of symmetric low molecular weight diblock copolymers in the vicinity of

the critical value for microphase separation was established to be in excellent agreement with this quantity.

Supporting information

NMR spectra, GPC traces, DSC thermograms, TGA data and additional TEM images at lower magnification.

Acknowledgements

This work is supported by NanoNextNL, a micro- and nanotechnology consortium of the Government of the Netherlands and 130 partners. Vincent Voet is greatly acknowledged for providing helpful suggestions on earlier drafts of this manuscript. Beam time on the Dutch-Belgian Beamline (DUBBLE) of ESRF (Grenoble, France) has kindly been made available by NWO, and we would like to thank Wim Bras, Giuseppe Portale and Daniel Hermida-Merino for their experimental assistance.

References

1. Abetz, V.; Simon, P. F. W. *Adv. Polym. Sci.* **2005**, *189*, 125–212.
2. Abetz, V. *Macromol. Rapid Commun.* **2015**, *36*, 10–22.
3. Voet, V. S. D.; Pick, T. E.; Park, S.; Moritz, M.; Hammack, A. T.; Urban, J. J.; Ogletree, D. F.; Olynick, D. L.; Helms, B. A. *J. Am. Chem. Soc.* **2011**, *133*, 2812–2815.
4. Koo, K.; Ahn, H.; Kim, S.; Ryu, D. Y.; Russell, T. P. *Soft Matter* **2013**, *9*, 9059–9071.
5. Park, W. I.; Kim, J. M.; Jeong, J. W.; Jung, Y. S. *ACS Nano* **2014**, *8*, 10009–10018.
6. Crossland, E. J. W.; Kamperman, M.; Nedelcu, M.; Ducati, C.; Wiesner, U.; Smilgies, D. M.; Toombes, G. E. S.; Hillmyer, M. A.; Ludwigs, S.; Steiner, U.; Snaith, H. J. *Nano Lett.* **2009**, *9*, 2807–2812.
7. Warren, S. C.; Messina, L. C.; Slaughter, L. S.; Kamperman, M.; Zhou, Q.; Gruner, S. M.; DiSalvo, F. J.; Wiesner, U. *Science* **2008**, *320*, 1748–1752.
8. Kamperman, M.; Garcia, C. B. W.; Du, P.; Ow, H.; Wiesner, U. *J. Am. Chem. Soc.* **2004**, *126*, 14708–14709.
9. Vukovic, I.; Punzhin, S.; Vukovic, Z.; Onck, P.; De Hosson, J. T. M.; ten Brinke, G.; Loos, K. *ACS Nano* **2011**, *5*, 6339–6348.
10. van Zoelen, W.; Bondzic, S.; Fernández Landaluce, T.; Brondijk, J.; Loos, K.; Schouten, A. J.; Rudolf, P.; ten Brinke, G. *Polymer* **2009**, *50*, 3617–3625.
11. Lim, H. S.; Lee, J.; Walish, J. J.; Thomas, E. L. *ACS Nano* **2012**, *6*, 8933–8939.
12. Lo, T.; Chao, C.; Ho, R.; Georgopanos, P.; Avgeropoulos, A.; Thomas, E. L. *Macromolecules* **2013**, *46*, 7513–7524.
13. Hückstädt, H.; Göpfert, A.; Abetz, V. *Macromol. Chem. Phys.* **2000**, *201*, 296–307.
14. Masuda, J.; Takano, A.; Suzuki, J.; Nagata, Y.; Noro, A.; Hayashida, K.; Matsushita, Y. *Macromolecules* **2007**, *40*, 4023–4027.
15. Asai, Y.; Yamada, K.; Yamada, M.; Takano, A.; Matsushita, Y. *ACS Macro Lett.* **2014**, *3*, 166–169.
16. Szwarc, M. *J. Polym. Sci. Part A: Polym. Chem.* **1998**, *36*, 9–15.
17. Baskaran, D.; Müller, A. H. E. *Prog. Polym. Sci.* **2007**, *32*, 173–219.
18. Hirao, A.; Goseki, R.; Ishizone, T. *Macromolecules* **2014**, *47*, 1883–1905.
19. Matyjaszewski, K. *Macromolecules* **2012**, *45*, 4015–4039.
20. Hawker, C. J.; Bosman, A. W.; Harth, E. *Chem. Rev.* **2001**, *101*, 3661–3688.
21. Chiefari, J.; Chong, Y. K.; Ercole, F.; Krstina, J.; Jeffery, J.; Le, T. P. T.; Mayadunne, R. T. A.; Meijs, G. F.; Moad, C. L.; Moad, G.; Rizzardo, E.; Thang, S. H. *Macromolecules* **1998**, *31*, 5559–5562.

22. Perrier, S.; Takolpuckdee, P. *J. Polym. Sci. Part A: Polym. Chem.* **2005**, *43*, 5347–5393.

23. Moad, G.; Rizzardo, E.; Thang, S. H. *Polymer* **2008**, *49*, 1079–1131.

24. Chong, B.; Le, T. P. T.; Moad, G.; Rizzardo, E.; Thang, S. H. *Macromolecules* **1999**, *32*, 2071–2074.

25. Mayadunne, R. T. A.; Rizzardo, E.; Chiefari, J.; Krstina, J.; Moad, G.; Postma, A.; Thang, S. H. *Macromolecules* **2000**, *33*, 243–245.

26. Convertine, A. J.; Sumerlin, B. S.; Thomas, D. B.; Lowe, A. B.; McCormick, C. L. *Macromolecules* **2003**, *36*, 4679–4681.

27. Zamfir, M.; Patrickios, C. S.; Montagne, F.; Abetz, C.; Abetz, V.; Oss-Ronen, L.; Talman, Y. *J. Polym. Sci. Part A: Polym. Chem.* **2012**, *50*, 1636–1644.

28. Yuan, J.; Ma, R.; Gao, Q.; Wang, Y.; Cheng, S.; Feng, L.; Fan, Z.; Jiang, L. *J. Appl. Polym. Sci.* **2003**, *89*, 1017–1025.

29. Wan, W.; Pan, C. *Polym. Chem.* **2010**, *1*, 1475–1484.

30. Božović-Vukić, J.; Mañon, H. T.; Meuldijk, J.; Koning, C.; Klumperman, B. *Macromolecules* **2007**, *40*, 7132–7139.

31. Jo, Y. S.; van der Vlies, A. J.; Gantz, J.; Antonijevic, S.; Demurtas, D.; Velluto, D.; Hubbell, J. A. *Macromolecules* **2008**, *41*, 1140–1150.

32. Nykänen, A.; Nuopponen, M.; Laukkanen, A.; Hirvonen, S.; Rytelä, M.; Turunen, O.; Tenhu, H.; Mezzenga, R.; Ikkala, O.; Ruokolainen, J. *Macromolecules* **2007**, *40*, 5827–5834.

33. Thomas, D. B.; Convertine, A. J.; Myrick, L. J.; Scales, C. W.; Smith, A. E.; Lowe, A. B.; Vasilieva, Y. A.; Ayres, N.; McCormick, C. L. *Macromolecules* **2004**, *37*, 8941–8950.

34. Wong, K. H.; Davis, T. P.; Barner-Kowollik, C.; Stenzel, M. H. *Polymer* **2007**, *48*, 4950–4965.

35. Convertine, A. J.; Lokitz, B. S.; Vasileva, Y.; Myrick, L. J.; Scales, C. W.; Lowe, A. B.; McCormick, C. L. *Macromolecules* **2006**, *39*, 1724–1730.

36. Hofman, A. H.; Reza, M.; Ruokolainen, J.; ten Brinke, G.; Loos, K. *Macromolecules* **2014**, *47*, 5913–5925.

37. Lai, J. T.; Filla, D.; Shea, R. *Macromolecules* **2002**, *35*, 6754–6756.

38. Kobayashi, M.; Okuyama, S.; Ishizone, T.; Nakahama, S. *Macromolecules* **1999**, *32*, 6466–6477.

39. Brandrup, J.; Immergut, E. H.; Grulke, E. A.; Abe, A.; Bloch, D. R. *Polymer Handbook*, 4th ed.; John Wiley & Sons, Inc., 1999.

40. Borsboom, M.; Bras, W.; Cerjak, I.; Detollenaere, D.; Glastra van Loon, D.; Goedtkindt, P.; Konijnenburg, M.; Lassing, P.; Levine, Y. K.; Munneke, B.; Oversluizen, M.; van Tol, R.; Vlieg, E. *J. Synchrotron Rad.* **1998**, *5*, 518–520.

41. Bras, W.; Dolbnya, I. P.; Detollenaere, D.; van Tol, R.; Malfois, M.; Greaves, G. N.; Ryan, A. J.; Heeley, E. *J. Appl. Cryst.* **2003**, *36*, 791–794.

42. Keddie, D. J.; Moad, G.; Rizzardo, E.; Thang, S. H. *Macromolecules* **2012**, *45*, 5321–5342.

43. Matsen, M. W.; Bates, F. S. *Macromolecules* **1996**, *29*, 1091–1098.

44. Hamley, I. W.; Castelletto, V. *Prog. Polym. Sci.* **2004**, *29*, 909–948.

45. Noro, A.; Sageshima, Y.; Arai, S.; Matsushita, Y. *Macromolecules* **2010**, *43*, 5358–5364.

46. Hashimoto, T.; Shibayama, M.; Kawai, H. *Macromolecules* **1980**, *13*, 1237–1247.

47. Khandpur, A. K.; Förster, S.; Bates, S.; Hamley, I. W.; Ryan, A. J.; Bras, W.; Almdal, K.; Mortensen, K. *Macromolecules* **1995**, *28*, 8796–8806.

48. Lynd, N. A.; Meuler, A. J.; Hillmyer, M. A. *Prog. Polym. Sci.* **2008**, *33*, 875–893.

49. Noro, A.; Iinuma, M.; Suzuki, J.; Takano, A.; Matsushita, Y. *Macromolecules* **2004**, *37*, 3804–3808.

50. Bates, F. S. *Science* **1991**, *251*, 898–905.

51. Clarke, C. J.; Eisenberg, A.; La Scala, J.; Rafailovich, M. H.; Sokolov, J.; Li, Z.; Qu, S.; Nguyen, D.; Schwarz, S. A.; Strzhemechny, Y.; Sauer, B. B. *Macromolecules* **1997**, *30*, 4184–4188.

52. Schubert, D. W.; Stamm, M.; Müller, A. H. E. *Polym. Eng. Sci.* **1999**, *39*, 1501–1507.

53. Zhao, Y.; Sivaniah, E.; Hashimoto, T. *Macromolecules* **2008**, *41*, 9948–9951.

54. Ludwigs, S.; Böker, A.; Abetz, V.; Müller, A. H. E.; Krausch, G. *Polymer* **2003**, *44*, 6815–6823.

55. Oudhuis, A. A. C. M.; ten Brinke, G.; Karasz, F. E. *Polymer* **1993**, *34*, 1991–1994.

56. Alberda van Ekenstein, G. O. R.; Meyboom, R.; ten Brinke, G.; Ikkala, O. *Macromolecules* **2000**, *37*, 3752–3756.

57. Gobius du Sart, G.; Rachmawati, R.; Voet, V.; Alberda van Ekenstein, G.; Polushkin, E.; ten Brinke, G.; Loos, K. *Macromolecules* **2008**, *41*, 6393–6399.

58. Gobius du Sart, G.; Vukovic, I.; Alberda van Ekenstein, G.; Polushkin, E.; Loos, K.; ten Brinke, G. *Macromolecules* **2010**, *43*, 2970–2980.

59. Scott, R. L. *J. Polym. Sci.* **1952**, *9*, 423–432.

60. Kambour, R. P.; Bendler, J. T.; Bopp, R. C. *Macromolecules* **1983**, *16*, 753–757.

61. ten Brinke, G.; Karasz, F. E.; MacKnight, W. J. *Macromolecules* **1983**, *16*, 1827–1832.

62. Bosma, M.; ten Brinke, G.; Ellis, T. S. *Macromolecules* **1988**, *21*, 1465–1470.

63. Grooten, R.; ten Brinke, G. *Macromolecules* **1989**, *22*, 1761–1766.

64. Sioula, S.; Hadjichristidis, N.; Thomas, E. L. *Macromolecules* **1998**, *31*, 5272–5277.

For Table of Contents use only